Supplementary Materials for

Water-induced dynamic $Zn_3(OH)_3$ complexes for complete CO_2 to methanol conversion on CuZn catalysts

Yunjian Ling[1,3,5], Wenjie Liao[2,5], Jun Cai[1,5], Jiayu Lv[1,5], Xiangxue Luo[1], Ruochen Liu[1], Weipeng Shao[1], Yihui Ren[1], Yuxi Huang[1], Shui Lin[1], Xiaofan Yu[1], Hui Zhang[4], Xinhe Bao[3], Zhi Liu[1]*, José A. Rodriguez[2]*, Ping Liu[2]*, Fan Yang[1,3]*

Affiliations:

[1]School of Physical Science and Technology, Center for Transformative Science, Shanghai Key Laboratory of High-resolution Electron Microscopy, ShanghaiTech University, Shanghai 201210, China.

[2]Chemistry Division, Brookhaven National Laboratory, Upton, New York 11973, United States.

[3]State Key Laboratory of Catalysis, Dalian Institute of Chemical Physics, Chinese Academy of Sciences, Dalian 116023, China.

[4]Shanghai Synchrotron Radiation Facility, Zhangjiang Laboratory, Shanghai Advanced Research Institute, Chinese Academy of Sciences, Shanghai 201204, China.

[5]These authors contributed equally: Yunjian Ling, Wenjie Liao, Jun Cai, Jiayu Lv.

*Corresponding authors. Email: liuzhi@shanghaitech.edu.cn (Z. L.); rodrigez@bnl.gov (J.A.R.); pingliu3@bnl.gov (P.L.); fyang@shanghaitech.edu.cn (F.Y.).

Table of Contents

Other Supplementary Materials for this manuscript include the following:

Supplementary Videos 1-2

Supplementary Note

Note 1. CuZn alloy surfaces in 5 bar $CO_2/H_2/H_2O$ with various Zn coverages

Upon exposure of a 0.2 ML Zn/Cu(111) surface to 5 bar of $CO_2/H_2/H_2O$ at 300 K, surface coarsening occurred through Zn oxidation processes, characterized by the nucleation of ZnO_x clusters (Supplementary Fig. 5B). At above 450 K, the Cu terraces became clean and smooth, accompanying the disappearances of clusters or nanolayers (Supplementary Fig. 5C). Between 473 and 550 K, the step edges fluctuated drastically (Supplementary Fig. 5D-E). Highly diffusive complexes or atoms in and out of the Cu steps appeared as spikes in STM images. When the CuZn alloy surface was cooled in reactant gas, the formation of ZnO islands could be observed (Supplementary Fig. 5F), likely through the coalescence of Zn_3-based complexes upon the decomposition/desorption of their ligands.

In 5 bar $CO_2/H_2/H_2O$, the Zn/Cu(111) surface with 0.4 ML Zn coverage showed similar surface features at 300 K (Supplementary Fig. 6B). Growth of two-dimensional (2D) ZnO islands emerged at 400 K (Supplementary Fig. 6C), progressing to three-dimensional (3D) ZnO particle formation at above 473 K (Supplementary Fig. 6D). Cu surface steps decorated with 3D ZnO particles displayed minimal step fluctuations. Similar to the CuZn alloy surface with 0.2 ML Zn coverage, cooling in reactant gases induced the reappearance of ZnO nanolayers (Supplementary Fig. 6F). However, the coverage of 2D ZnO nanolayers is much less than that on the 0.2 ML Zn/Cu(111) surface after reaction, indicating a diminished presence of Zn complexes during CO_2 hydrogenation reactions.

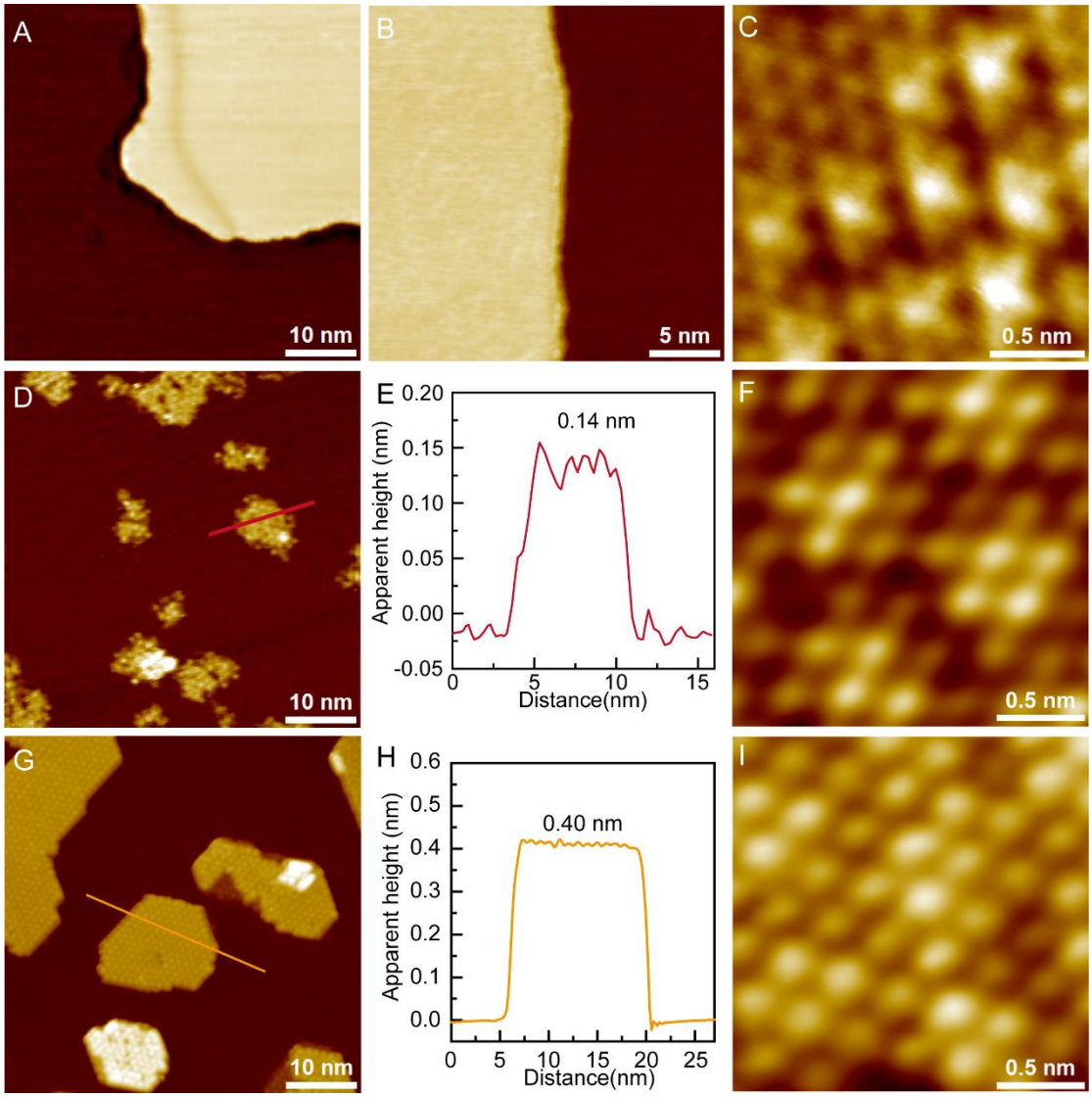

Supplementary Fig. 1 | STM images of CuZn alloy and ZnO/Cu model catalysts. (A) STM image of Zn/Cu(111) surface prepared by depositing Zn atoms in UHV onto Cu(111) at 300 K. (B) CuZn alloy surface prepared by flashing the Zn/Cu(111) surface to 450 K. (C) Atomic-resolution STM image of the CuZn alloy surface. (D) STM image of ZnO/Cu interface with dominantly monolayer g-ZnO islands prepared by oxidizing the CuZn alloy surface in 1 mbar CO_2 at 450 K, followed by annealing in UHV at 500 K, and (E) corresponding height profile along the red line in (D). (F) Atomic resolution STM image of the monolayer g-ZnO layer surface with 3.3 Å lattice spacing. (G) STM image of ZnO/Cu interface with dominantly bilayer g-ZnO islands prepared by evaporating Zn atoms in 10^{-6} mbar O_2 onto Cu(111) at 300 K, followed by annealing in 10^{-6} mbar O_2 at 500 K, and (H) corresponding height profile along the yellow line in (G). (I) Atomic-resolution STM image of the bilayer g-ZnO layer surface with 3.3 Å lattice spacing.

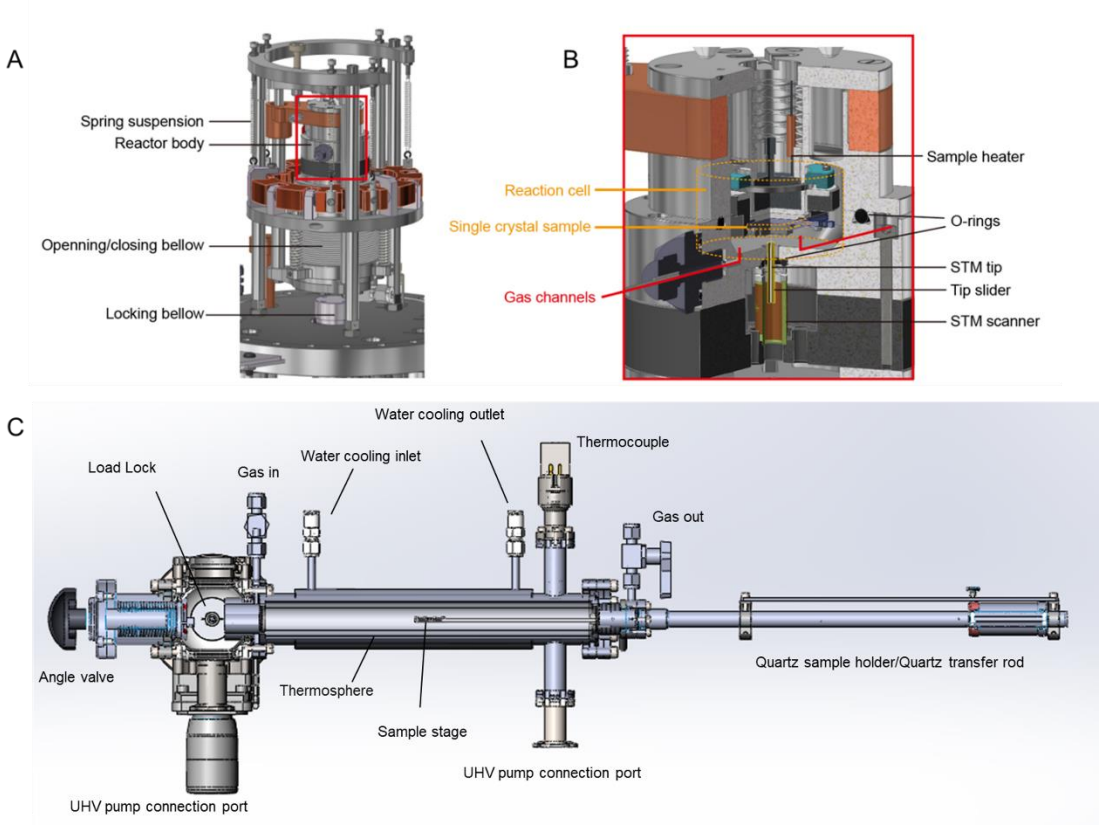

Supplementary Fig. 2 | Schematics of HP reactor STM and high-pressure quartz reactor. (A) Schematics of HP reactor STM supported on a UHV flange. The reactor STM head is marked by a red rectangle and its cross-sectional diagram is enlarged in (B). (C) The cross-sectional diagram of a high-pressure quartz reactor, which is UHV compatible and has a working pressure range up to 1 MPa.

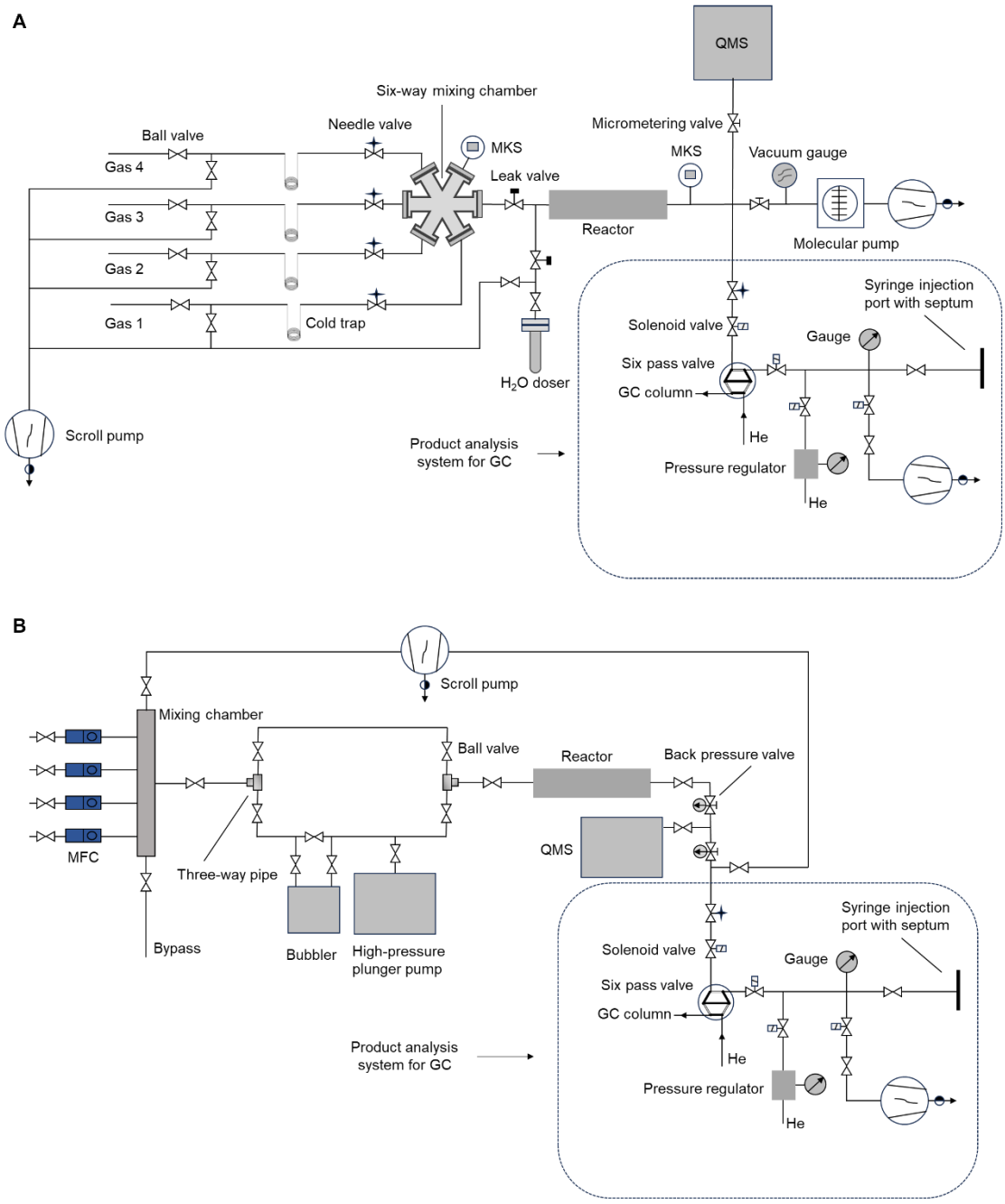

Supplementary Fig. 3 | Gas supply and reaction analysis systems. (A) Gas supply system for ambient-pressure reaction kinetics measurements. (B) Gas supply system for high-pressure (1-10 bar) reaction kinetics measurements.

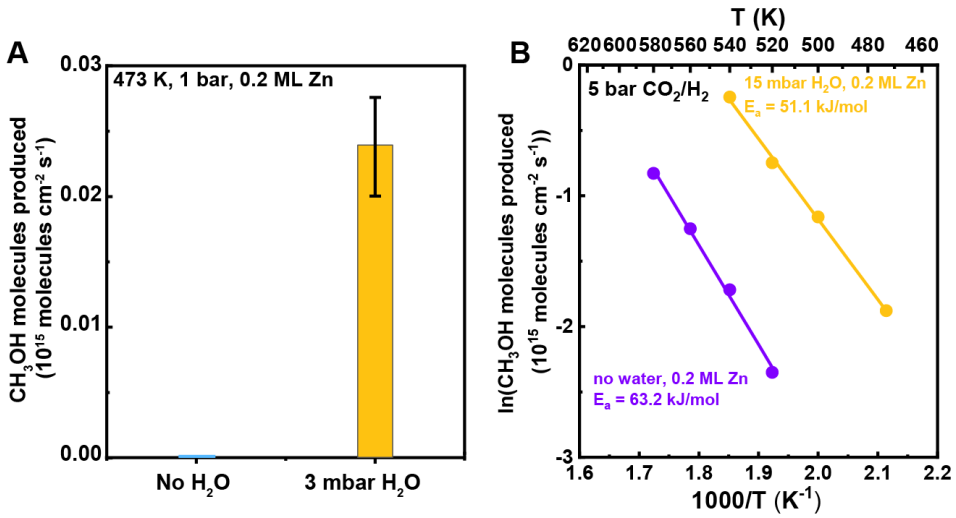

Supplementary Fig. 4 | Comparison of methanol formation rates under anhydrous and hydrous conditions. (A) Methanol formation rates on 0.2 ML Zn/Cu(111) under anhydrous and hydrous (3 mbar H_2O) conditions at 473 K, in 1 bar CO_2/H_2 mixture gas (p_{CO_2} = 0.25 bar, p_{H_2} = 0.75 bar). (B) Arrhenius plots for methanol formation via CO_2 hydrogenation on 0.2 ML Zn/Cu(111) in 5 bar $CO_2/H_2/H_2O$ mixture gas (p_{CO_2} = 1.25 bar, p_{H_2} = 3.75 bar, p_{H_2O} = 0 or 15 mbar).

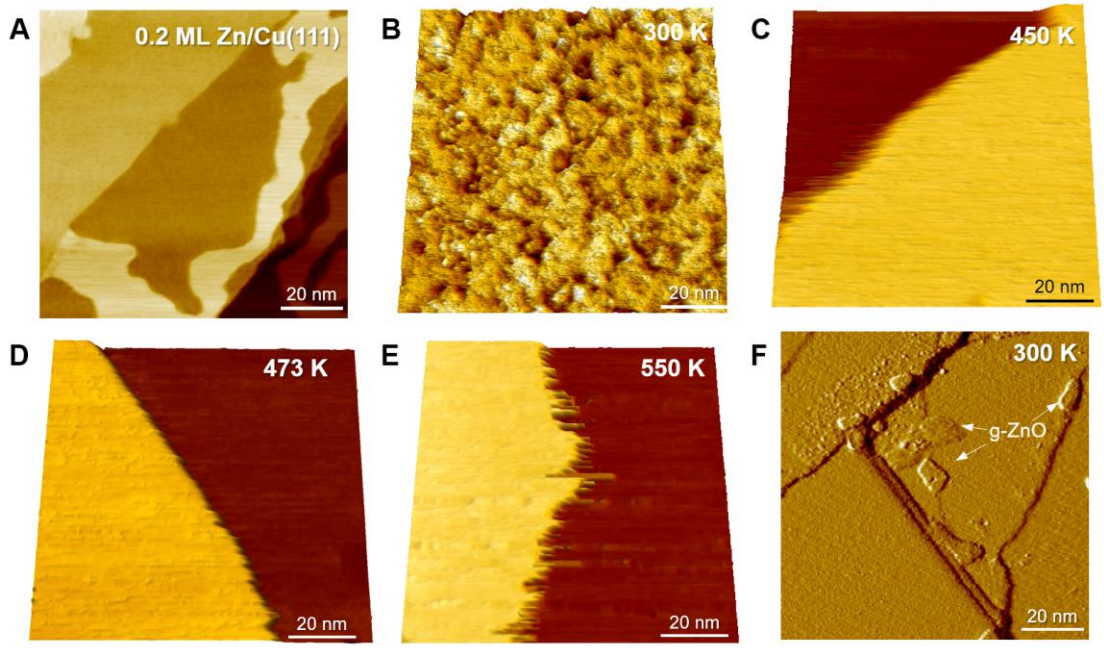

Supplementary Fig. 5 | High-pressure STM of CuZn alloy surface in 5 bar $CO_2/H_2/H_2O$. (A) Large-scale STM image of a 0.2 ML Zn/Cu(111) surface. (B-E) In-situ STM images in 5 bar $CO_2/H_2/H_2O$ (p_{CO_2} = 1.25 bar, p_{H_2} = 3.75 bar, p_{H_2O} = 15 mbar) at 300, 450, 473, and 550 K, showing clean Cu terraces with step fluctuations. (F) Post-reaction image showing g-ZnO islands near Cu(111) steps at 300 K. The g-ZnO islands were formed during the cooling under reaction atmosphere.

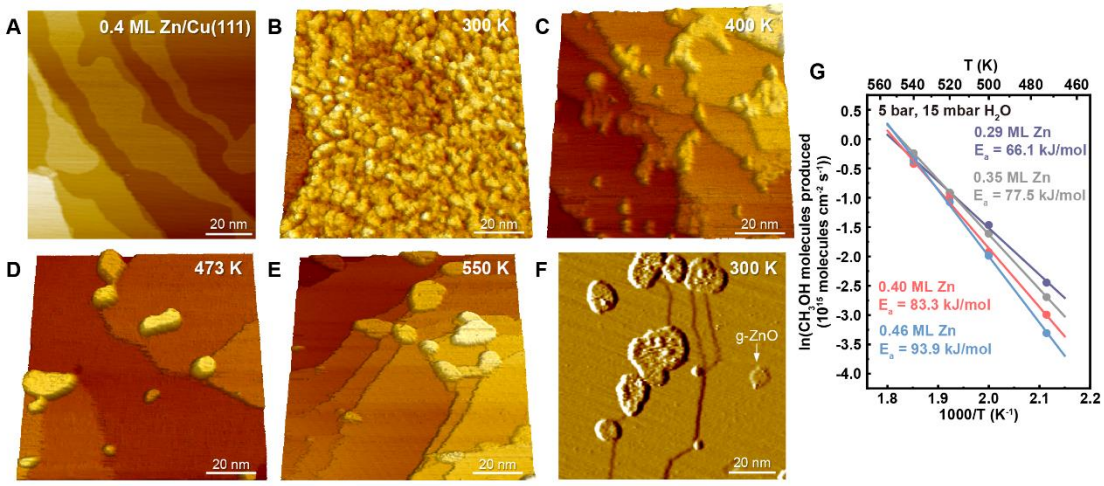

Supplementary Fig. 6 | High-pressure STM of high-coverage Zn/Cu(111) and apparent activation energies of methanol formation in 5 bar $CO_2/H_2/H_2O$. (A) Large-scale STM image of a 0.4 ML Zn/Cu(111) surface. (B-E) HP-STM images in 5 bar $CO_2/H_2/H_2O$ (p_{CO_2} = 1.25 bar, p_{H_2} = 3.75 bar, p_{H_2O} = 15 mbar) at 300, 400, 473, and 550 K showing surface evolution. The CuZn alloy surface (B) becomes coarser due to Zn oxidation and the formation of ZnO_x clusters at 300 K, which turned into (C) g-ZnO nanolayers at 400 K. (D) g-ZnO islands decomposed at 500 K, accompanying the emergence of 3D-ZnO on the surface. (E) 3D-ZnO remained stable at 550 K. (F) Post-reaction image showing a g-ZnO island formed during the cooling under reaction atmosphere. (G) Arrhenius plots of methanol formation via CO_2 hydrogenation on Zn/Cu(111) surfaces with θ_{Zn} > 0.2 ML in 5 bar $CO_2/H_2/H_2O$ mixture gas (p_{CO_2} = 1.25 bar, p_{H_2} = 3.75 bar, p_{H_2O} = 15 mbar).

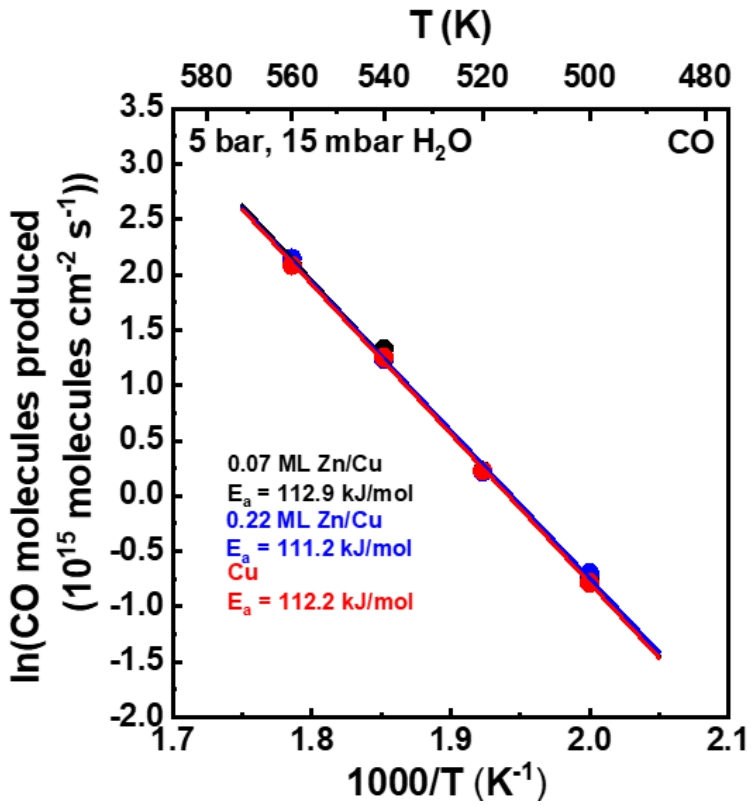

Supplementary Fig. 7 | Arrhenius plots of CO formation via CO_2 hydrogenation on 0.07, 0.22 ML Zn/Cu(111) and Cu(111) surfaces in 5 bar $CO_2/H_2/H_2O$ mixture gas (p_{CO_2} = 1.25 bar, p_{H_2} = 3.75 bar, p_{H_2O} = 15 mbar).

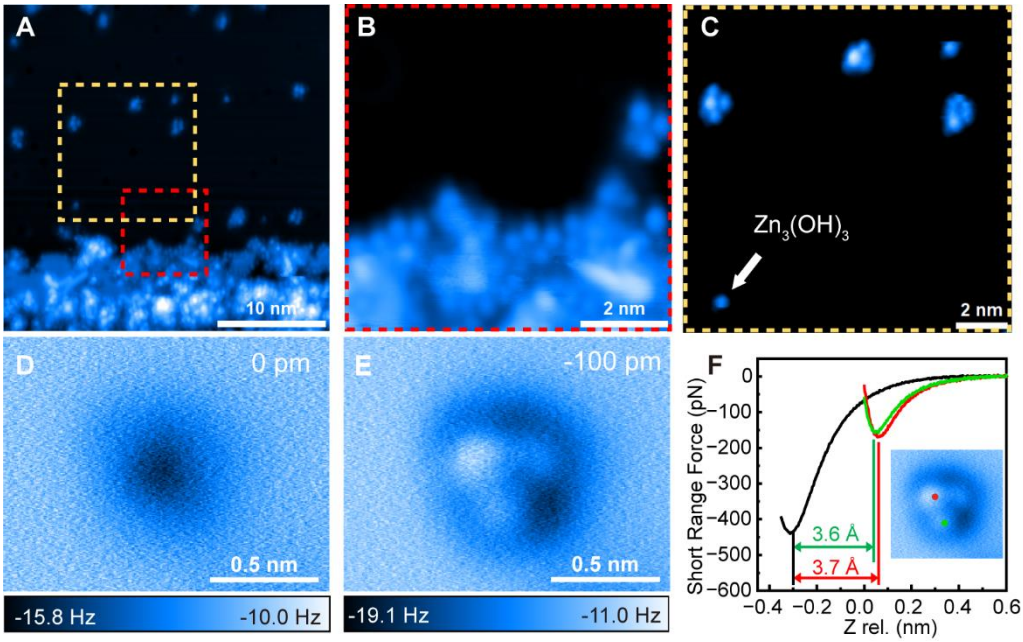

Supplementary Fig. 8 | Formation of Zn_3-based complexes after exposing the CuZn alloy surface to 5 bar $CO_2/H_2/H_2O$ at 550 K. (A) Large-scale STM image showing formation of Zn_3-based complexes on CuZn alloy surface after reaction in 5 bar $CO_2/H_2/H_2O$ (p_{CO_2} = 1.25 bar, p_{H_2} = 3.75 bar, p_{H_2O} = 15 mbar) at 550 K. (B,C) Magnified STM images of cluster distribution at (B) step edges (yellow dashed box in A) and (C) terraces (red dashed box in A). (D-E) Constant-height AFM images confirming the formation of $Zn_3(OH)_3$ after reaction in 5 bar $CO_2/H_2/H_2O$ (p_{CO_2} = 1.25 bar, p_{H_2} = 3.75 bar, p_{H_2O} = 15 mbar) at 550 K. The tip heights of AFM images are 0 pm, -100 pm, respectively, which are referenced to the STM set point on Cu(111). Scanning parameters: V_s = 100 mV; I_t = 20 pA. (F) Short-range force-distance curves for Cu(111) (black), higher OH group (red) and lower OH group (green).

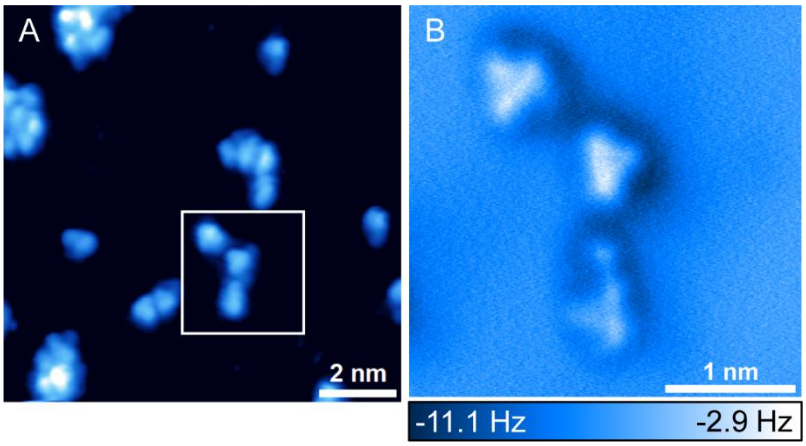

Supplementary Fig. 9 | Formation of clusters with structural moiety of Zn trimers after exposing the Zn/Cu(111) surface to 5 bar $CO_2/H_2/H_2O$ (p_{CO_2} = 1.25 bar, p_{H_2} = 3.75 bar, p_{H_2O} = 15 mbar) at 550 K. (A) STM image showing formation of Zn_3-based complexes on Cu terraces. Scanning parameters: V_s = -50 mV; I_t = 10 pA. (B) The magnified AFM image (white box in A) confirms the clusters consist of Zn_3 moiety. The tip height (+75 pm) of AFM images is referenced to the STM image set point on Cu(111). Scanning parameters: V_s = -50 mV; I_t = 10 pA.

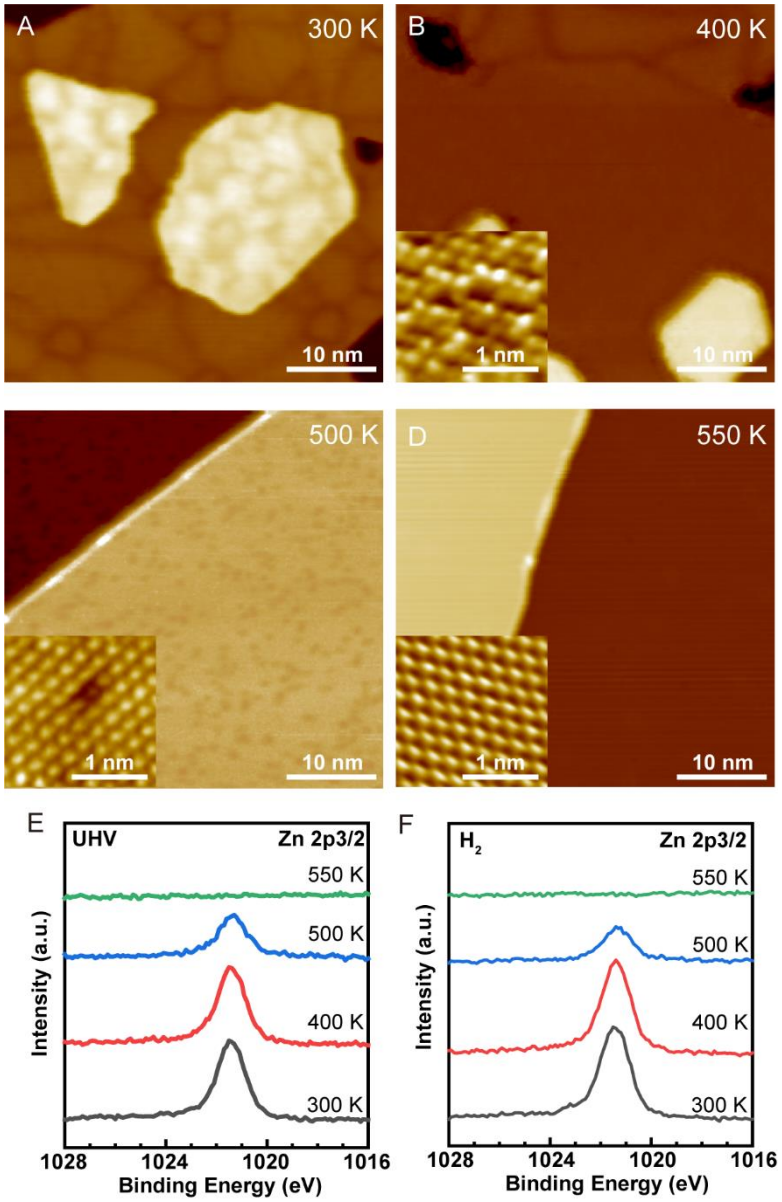

Supplementary Fig. 10 | Thermal stability analysis of Zn atoms in the CuZn alloy surface under UHV and H_2 atmosphere. STM images of 2 ML Zn/Cu(111) surfaces (A) as-deposited at 300 K, followed by annealing at (B) 400 K, (C) 500 K, and (D) 550 K, with atomic-resolution insets. (E-F) XPS Zn 2p3/2 spectra of Zn/Cu(111) under (E) UHV or (F) 0.5 mbar H_2 at elevated temperatures.

The CuZn alloy surface was prepared by UHV deposition of Zn atoms onto Cu(111), intermixing of Zn with the Cu layer was observed at 400 K. Insets revealed Zn atom substitution within the Cu(111) lattice, manifesting as bright protrusions. Due to the different atomic radius of Zn and Cu, the intermixing induced lattice distortion and stacking faults between atomic layers. Analogous to the herringbone reconstruction observed on Au(111)[1], the depressed-line structures in the alloying region likely originated from these stacking fault configurations. Upon annealing at 400 K, the depressed-line structures and hexagonal islands decreased on surfaces and homogeneously distributed Zn atoms were observed within the Cu(111) lattice,

indicating a uniform CuZn alloy surface. Subsequent annealing at 500 K resulted in surface restoration to a Cu(111) lattice with dark spots, suggesting Zn atom evaporation. Complete Zn evaporation was confirmed at 550 K, as indicated by the disappearance of dark surface features in STM and loss of Zn 2p3/2 intensity in XPS.

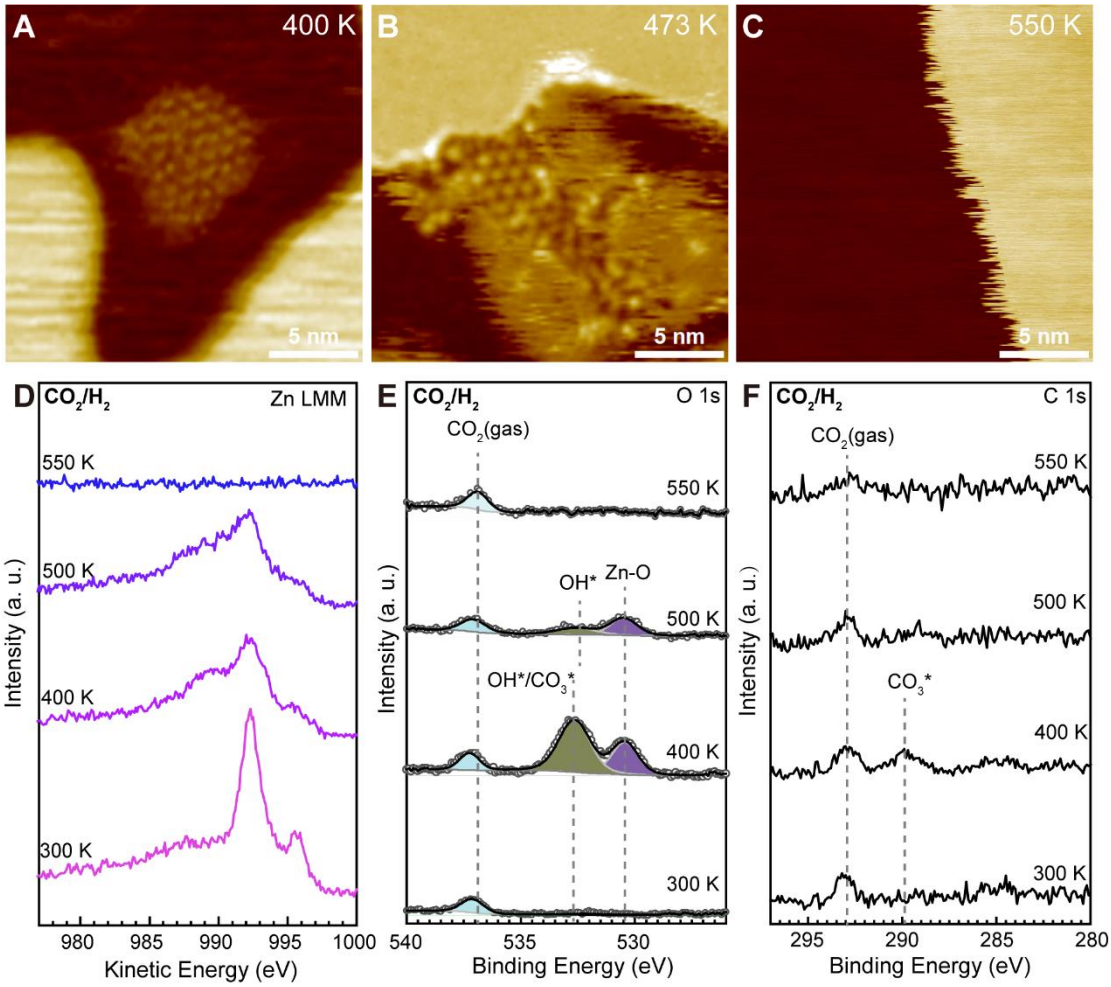

Supplementary Fig. 11 | Thermal stability analysis of CuZn alloy under CO_2/H_2 atmospheres at elevated temperatures. AP-STM images showing morphological evolution in 0.25 mbar CO_2 and 0.75 mbar H_2. (A) g-ZnO nanolayer formation at 400 K, (B) subsequent reduction at 473 K, and (C) metallic nanolayer disappearance at 550 K. (D-F) XPS spectra (Zn LMM, O 1s, and C 1s) of the CuZn alloy surface under 0.25 mbar CO_2 and 0.75 mbar H_2 at elevated temperatures.

In 0.25 mbar CO_2 and 0.75 mbar H_2, two-dimensional (2D) ZnO nanolayers emerged on CuZn alloy surface at 400 K. The 2D ZnO nanolayers were partially reduced at 473 K, but would be completely reduced at 550 K, leaving clean surfaces and fluctuated step edges. Consistently, AP-XPS measurements confirmed the formation of ZnO at 400 K by the emergence of O 1s peak at 530.4 eV and Zn LMM peak at 988.5 eV. In 1 mbar CO_2/H_2, the CuZn alloy could not be fully oxidized, evidenced by the existence of Zn LMM peak at 992.3 eV from 300 K to 500 K. Accompanied by desorption of carbonates at 500 K, complete reduction of ZnO and Zn evaporation was confirmed at 550 K, as indicated by the loss of Zn LMM intensity.

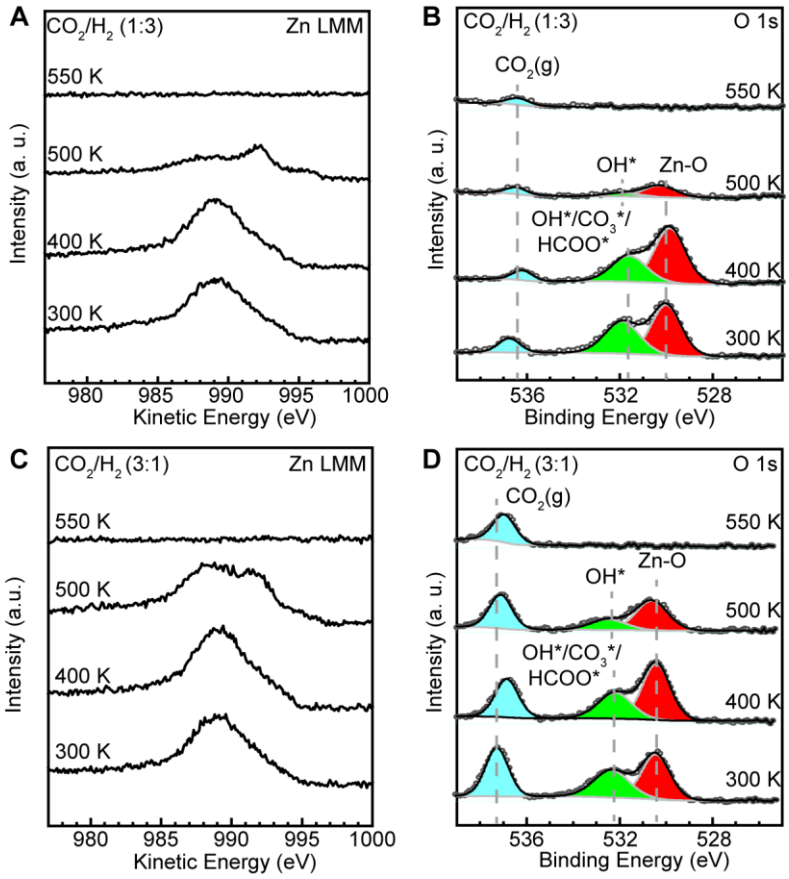

Supplementary Fig. 12 | Thermal stability analysis of ZnO nanolayers under CO_2/H_2 atmospheres with various ratios at elevated temperatures. (A-B) XPS Zn LMM and O 1s spectra of the g-ZnO/Cu(111) surface under 0.5 mbar CO_2 and 1.5 mbar H_2 at elevated temperatures. (C-D) XPS Zn LMM and O 1s spectra of the g-ZnO/Cu(111) surface under 1.5 mbar CO_2 and 0.5 mbar H_2 at elevated temperatures. AP-XPS measurements demonstrated the thermal instability of these g-ZnO islands in CO_2/H_2 environments with various ratios at 500 K, with complete reduction and Zn evaporation occurring at 550 K.

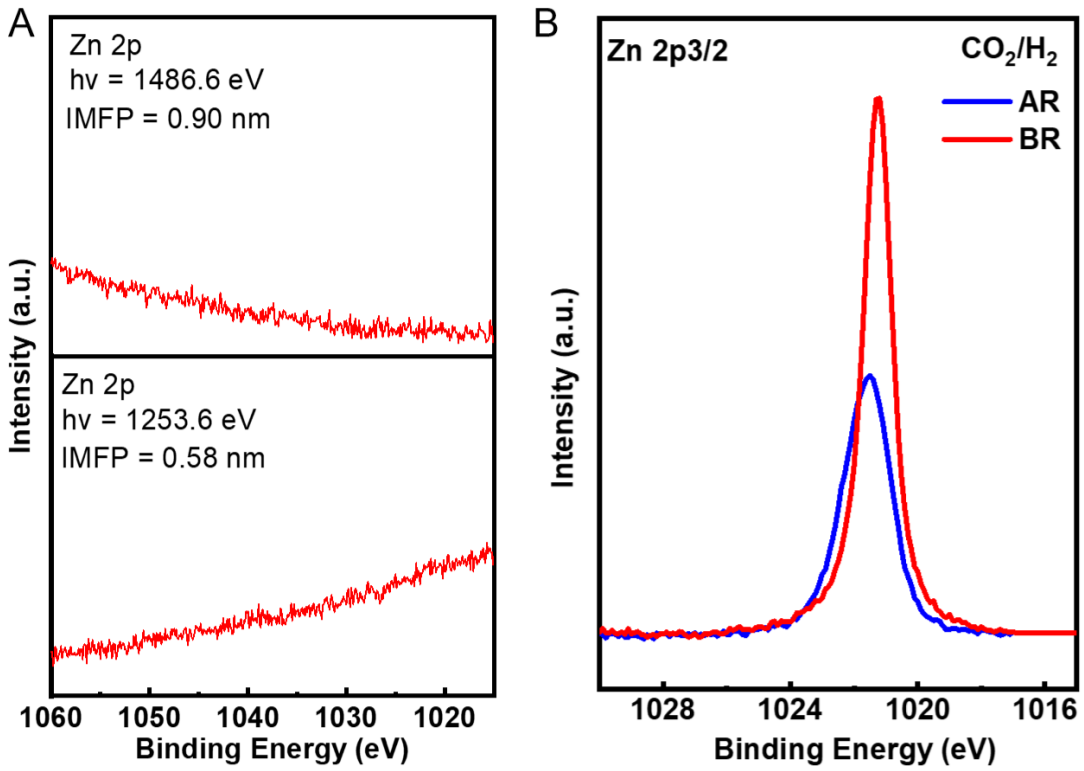

Supplementary Fig. 13 | Depth-dependent spectral analysis of XPS Zn 2p signal and thermal stability analysis of CuZn alloy under 5 bar CO_2/H_2 atmospheres. (A) With different incident photon energies, the background trend of inelastic scattering electrons is different. XPS Zn 2p spectra were acquired at two photon energies, 1253.6 eV and 1486. 6eV, yielding detection depths of 2.7 nm and 1.74 nm, respectively. These depths were defined using three times the inelastic mean free path (IMFP). XPS Zn 2p spectra showed no peak was observed on the CuZn alloy surface after reaction in 0.25 mbar CO_2 and 0.75 mbar H_2 at 550 K, confirming the complete Zn volatilization. (B) XPS Zn 2p3/2 spectra of CuZn alloy surface before and after reaction in 1.25 bar CO_2 and 3.75 bar H_2 at 550 K, showing the loss of Zn without water.

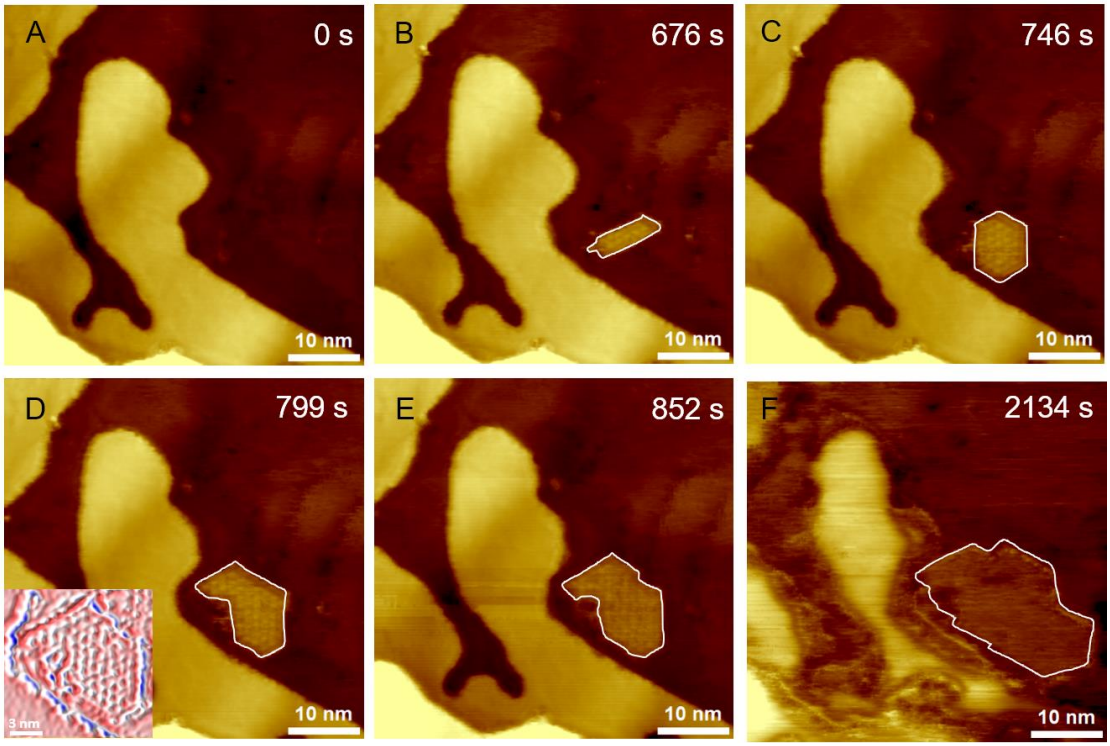

Supplementary Fig. 14 | In situ AP-STM analysis of Zn/Cu(111) alloy oxidation by H_2O. (A-E) Sequential in situ AP-STM images tracking CuZn alloy terrace reduction and ZnO nanolayer growth under 1×10^{-4} mbar H_2O at 300 K at 0, 676, 746, 799 and 852 s. The smallest g-ZnO island observed displayed a width of ~ 2 nm. (F) Subsequent image increasing pressure to 1 mbar at 2134 s. Solid white lines indicate the expanding ZnO islands during reaction process. Inset image in (D) shows the high-resolution STM image of ZnO nanolayer island. Scanning parameters: V_s = -1.01 V; I_t = 204 pA.

$$3Zn + 3H_2O \rightarrow Zn_3(OH)_3 + 3/2H_2$$

$$Zn_3(OH)_3 \rightarrow Zn_3O_3 + 3/2H_2$$

$$xZn_3O_3 \rightarrow (ZnO)_{3x}$$

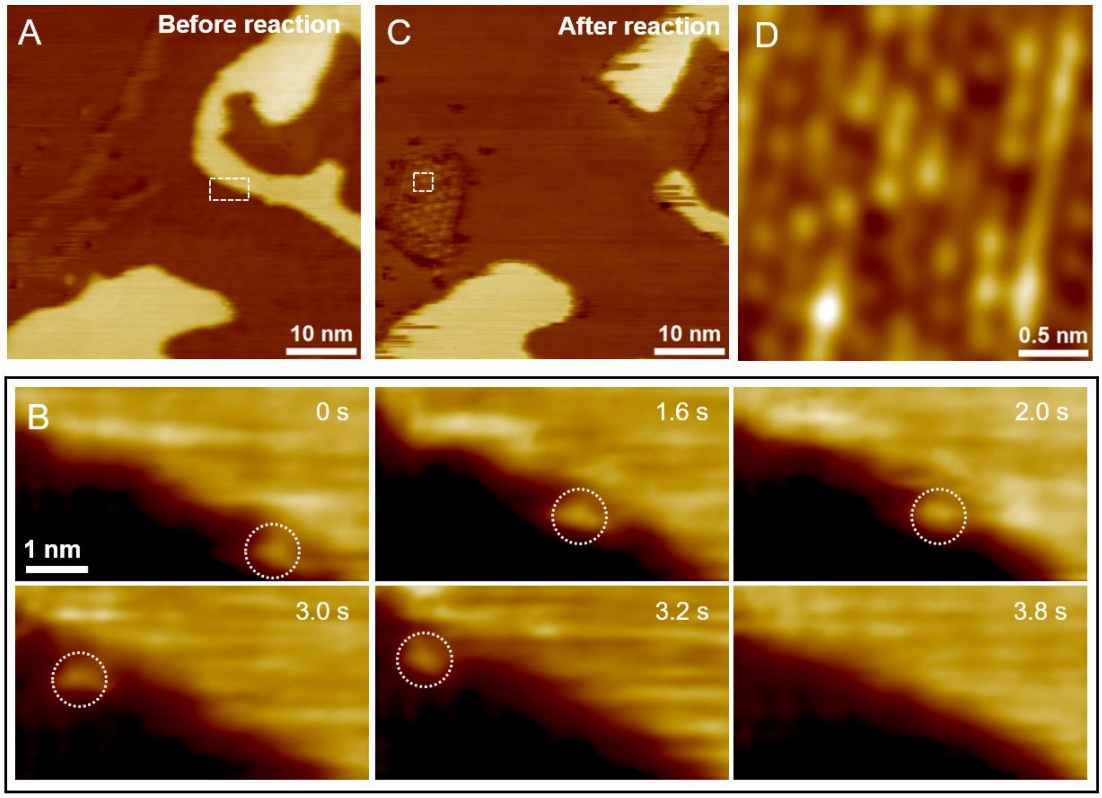

Supplementary Fig. 15 | High-speed STM analysis of Zn/Cu(111) surfaces under H_2O exposure. (A) STM image of as-prepared Zn/Cu(111), with high-speed scan region marked by white dashed box. (B) Sequential high-speed STM images under 1×10^{-4} mbar H_2O showing the formation and migration of Zn_3-based complexes along step edges. Images are excerpted from Supplementary Video 2, with a scanning speed of 5 frames per second. (C) Post-reaction STM image showing partial dissolution of CuZn alloy layer and g-ZnO island formation near the CuZn alloy layer, with magnified high-resolution STM image (white dashed box in C) detailed in (D).

In situ STM observed the growth of ZnO on Cu terraces along with the formation of mobile Zn_3-based complexes in vacuum, suggesting that Zn_3-based complexes are only dynamically stabilized.

$$3Zn + 3H_2O \rightarrow Zn_3(OH)_3 + 3/2H_2$$

$$Zn_3(OH)_3 \rightarrow Zn_3O_3 + 3/2H_2$$

$$xZn_3O_3 \rightarrow (ZnO)_{3x}$$

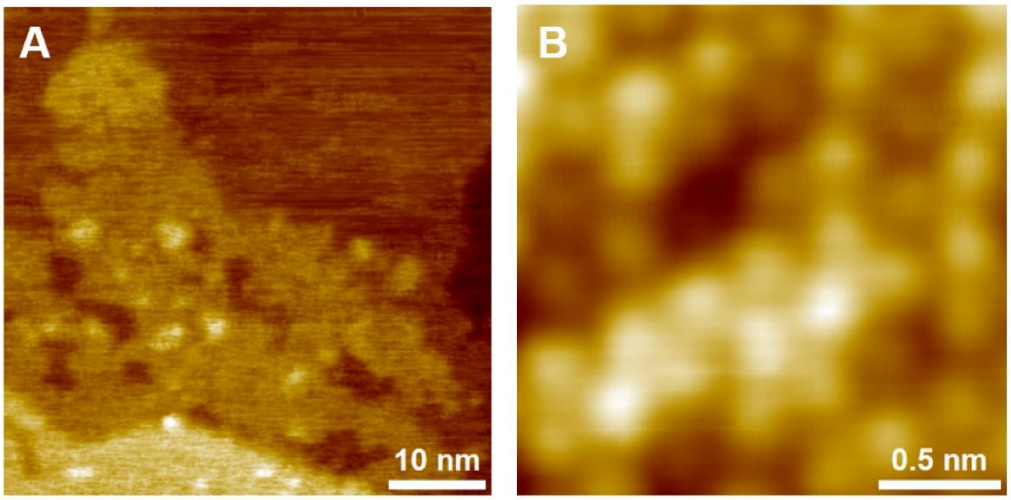

Supplementary Fig. 16 | Formation of hydroxylated ZnO islands after exposing the CuZn alloy surface to 1 mbar H_2O. (A) STM image in 1 mbar H_2O showing the disappearance of moire pattern on ZnO islands due to the dynamic H_2O adsorption. (B) STM image taken after water evacuation showing the atomic structure of the g-ZnO surface with 3.3 Å lattice spacing.

$$Zn_{3x}O_{3x} + yH_2O \rightarrow Zn_{3x}O_{3x-y}(OH)_{2y}$$

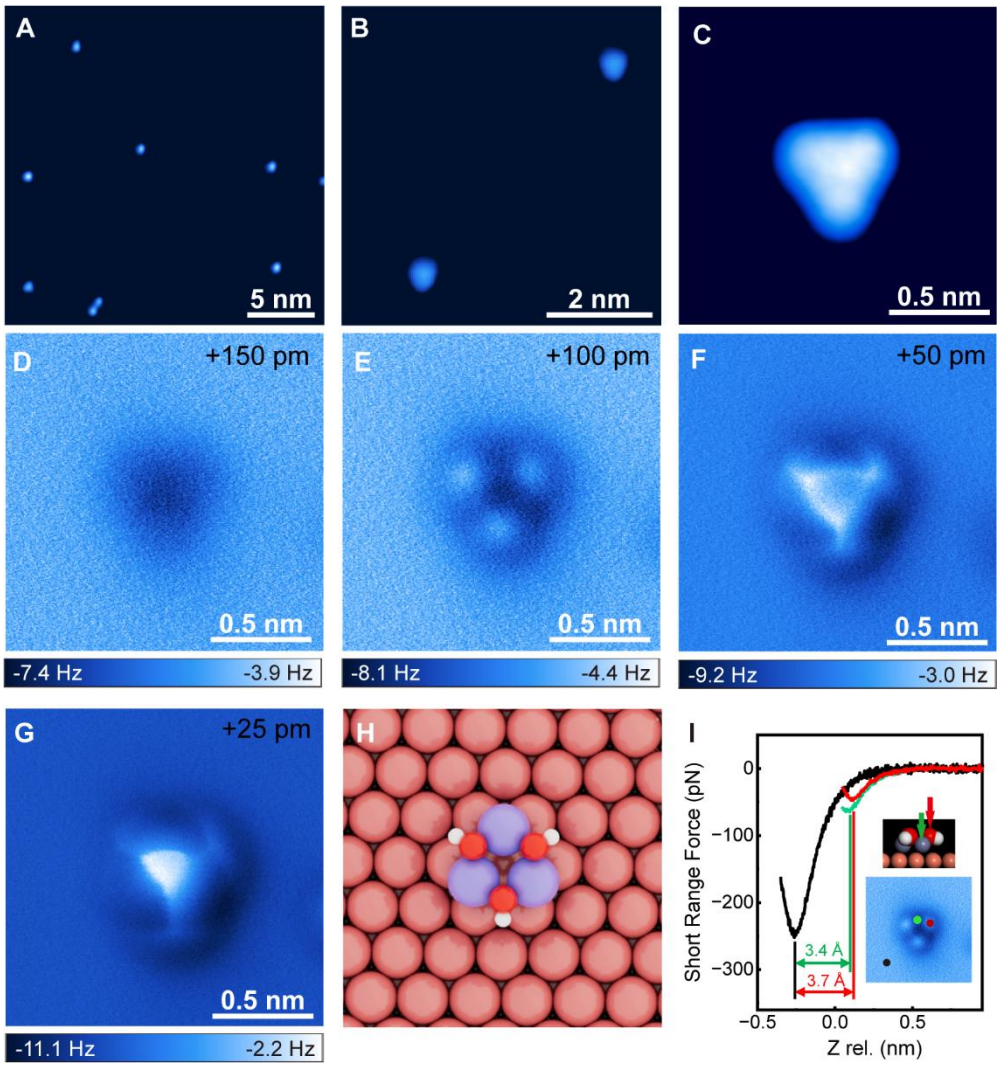

Supplementary Fig. 17 | Formation, distribution and identification of symmetric $Zn_3(OH)_3$ on Cu(111). (A) STM image showing formation of bright spots on Cu terraces after exposure to 5×10^{-6} mbar H_2O at 250 K. Scanning parameters: V_s = -1000 mV; I_t = 1.7 nA. (B) Magnified STM image of the bright spots, which are confirmed as $Zn_3(OH)_3$ clusters in (C-G). Scanning parameters: V_s = -100 mV; I_t = 20 pA. (C) STM and (D-G) constant-height AFM images of triple-symmetric $Zn_3(OH)_3$ at varying tip heights. The tip heights of AFM images are +150 pm, +100 pm, +50 pm, +25 pm, respectively, which are referenced to the STM set point on Cu(111). Scanning parameters: V_s = -200 mV; I_t = 30 pA. (H) DFT-optimized model of the $Zn_3(OH)_3$. Color code: Reddish-orange - Cu; Cyan - Zn; Red - O; White - H. (I) Short-range force-distance curves for Cu(111) (black), bridge OH group (red), and Zn (green).

$$3Zn + 3H_2O \rightarrow Zn_3(OH)_3 + 3/2H_2$$

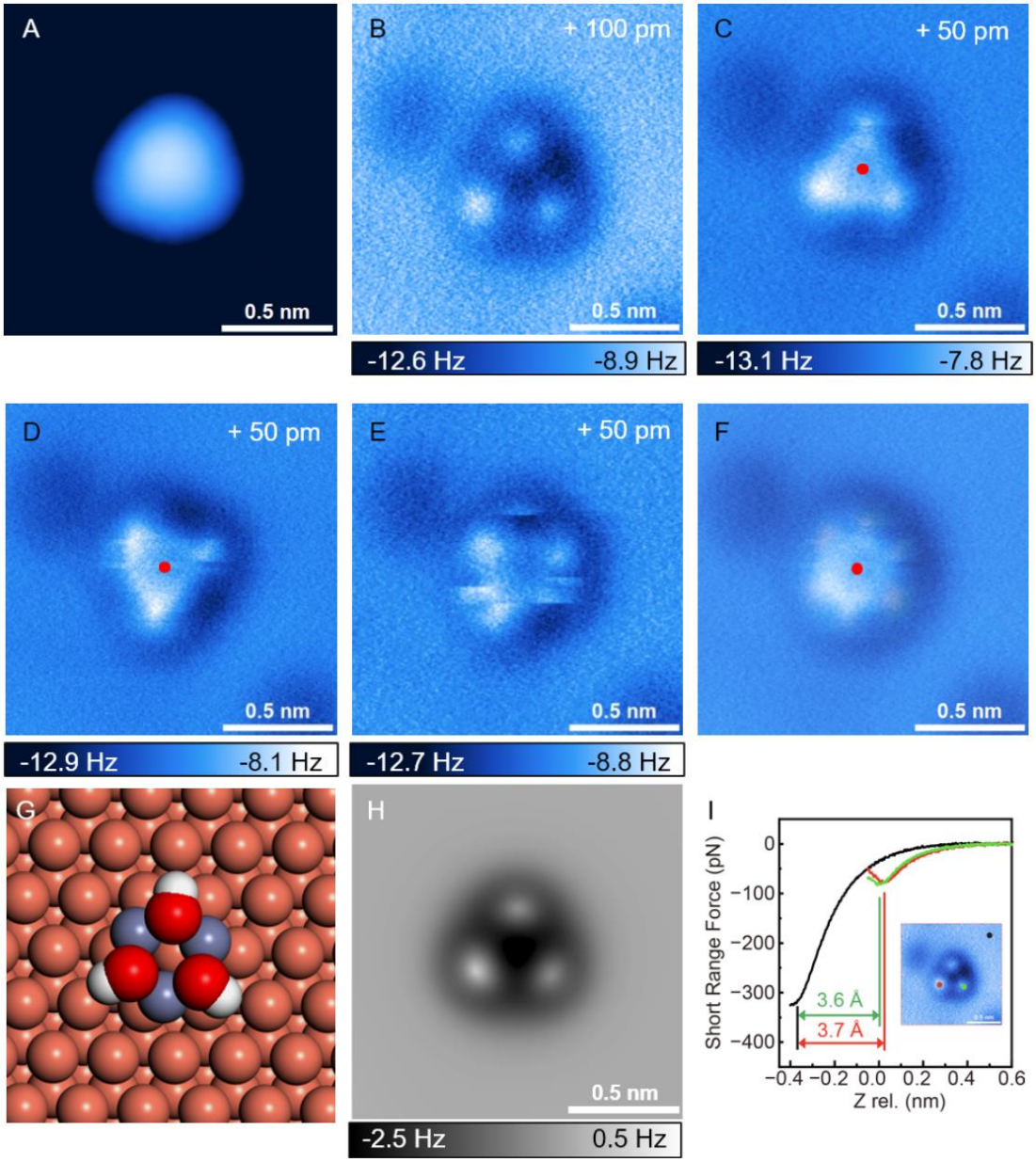

Supplementary Fig. 18 | Rotational mobility of $Zn_3(OH)_3$. (A) STM image of rotatable $Zn_3(OH)_3$, which appear asymmetric in their anchoring sites on Cu(111). The rotational mobility is exemplified by its fuzzy feature and (B,C) corresponding constant-height AFM images. The tip heights of AFM images are +100 pm and +50 pm, respectively, which are referenced to the STM set point on Cu(111). Scanning parameters: V_s = -200 mV; I_t = 100 pA. (D) AFM image showing an alternate angle after tip-induced rotation. (E) Single-scan sequence showing rotation-induced fuzzy lines. (F) Overlay of images (C) and (D). (G) Structural model and (H) AFM simulation of the asymmetric $Zn_3(OH)_3$. Color code: Coral - Cu; Grey - Zn; Red - O; White - H. (I) Short-range force-distance curves for Cu(111) (black), higher OH group (red) and lower OH group (green).

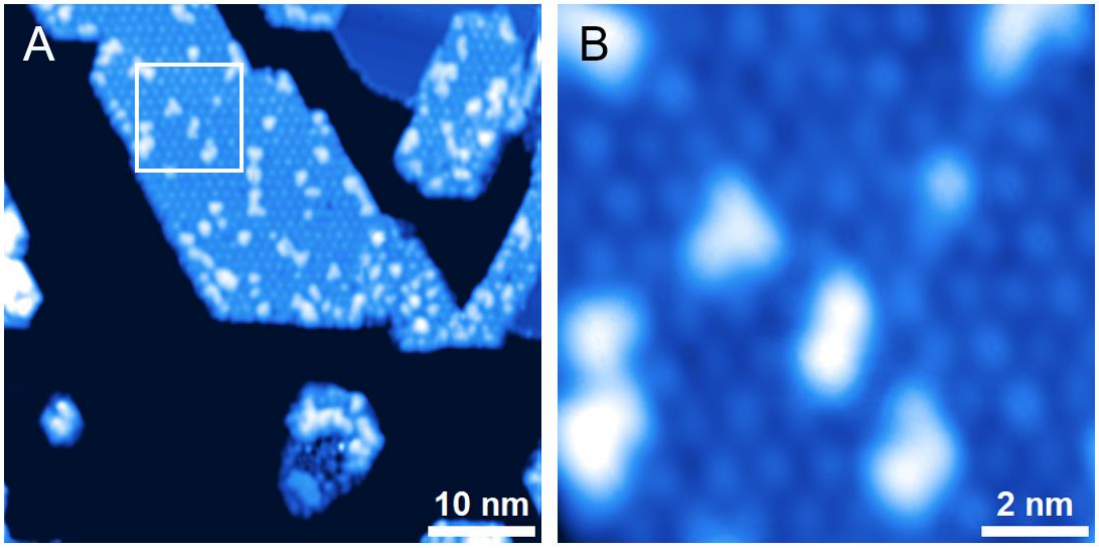

Supplementary Fig. 19 | Adsorption of H_2O on g-ZnO. (A) Large-scale and (B) magnified STM images of g-ZnO islands after exposing g-ZnO to 1×10^{-8} mbar H_2O water for 120 s at 110 K.

$$Zn_{3x}O_{3x} + yH_2O \rightarrow Zn_{3x}O_{3x-y}(OH)_{2y}$$

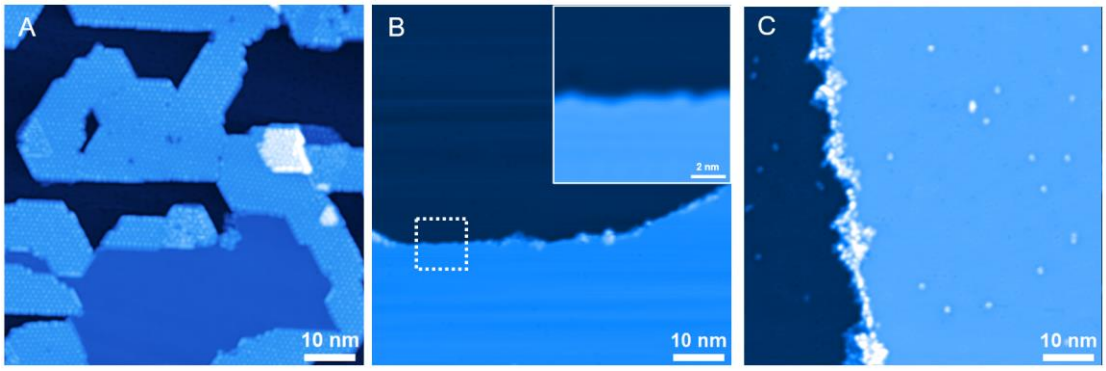

Supplementary Fig. 20 | H_2O stabilization effect on ZnO under atomic H exposure. (A) Large-scale STM image of g-ZnO islands on Cu(111). (B) STM images showing clean Cu(111) surface after g-ZnO reduction in 5×10^{-8} mbar atomic H at 550 K for 20 min. ZnO islands were fully reduced by atomic H, forming metallic Zn atoms which evaporated away from the Cu surface. Inset confirmed a clean Cu(111) lattice. (C) STM image of the g-ZnO/Cu interface after simultaneous exposure to 2.5×10^{-8} mbar H_2O and 5×10^{-8} mbar atomic H at 550 K for 20 min, followed by cooling in atmosphere, showing dispersion of clusters across the surface and enriched at Cu steps.

$$Zn_{3x}O_{3x-y}(OH)_{2y} + 3H \rightarrow Zn_3(OH)_3 + Zn_{3x-3}O_{3x-y-3}(OH)_{2y-3} + 3H_2O$$

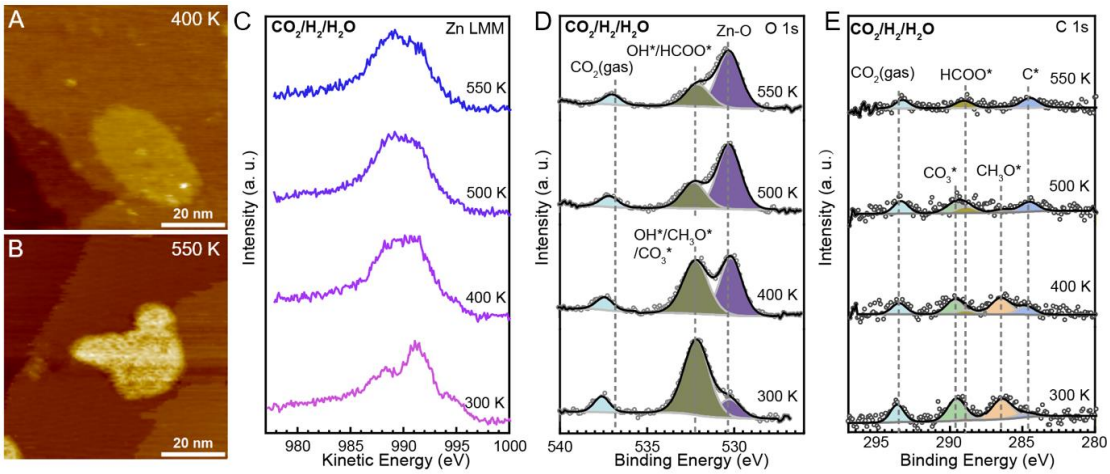

Supplementary Fig. 21 | Thermal stability analysis of the CuZn alloy surface under 1 mbar $CO_2/H_2/H_2O$ at elevated temperatures. (A-B) AP-STM images showing surface morphological evolution in 0.25 mbar CO_2, 0.75 mbar H_2, and 0.04 mbar H_2O with the formation of hydroxylated ZnO nanolayers (A) at 400 K and (B) the formation of 3D ZnO particles at 550 K. (C-E) AP-XPS Zn LMM, O 1s, and C 1s spectra of the CuZn alloy surface in 0.25 mbar CO_2, 0.75 mbar H_2, and 0.04 mbar H_2O at elevated temperatures.

In 0.25 mbar CO_2, 0.75 mbar H_2, and 0.04 mbar H_2O, hydroxylated two-dimensional (2D) ZnO nanolayers emerged on CuZn alloy surface at 400 K, and progressed to three-dimensional (3D) ZnO particle at 550 K. Consistently, AP-XPS measurements show the oxidation of metallic Zn at 300 K by the emergence of O 1s peak at 530.4 eV and Zn LMM peak at 988.5 eV. At 400 K, metallic Zn was fully oxidized, evidenced by the disappearance of a shoulder peak of Zn^0 at 995.0 eV and the concurrent increase of the Zn^{2+} peak at 988.5 eV. Above 500 K, minor change was observed in Zn LMM spectra, indicating the thermal stability of Zn species in hydrous conditions. In contrast to the case in the anhydrous condition (Supplementary Fig. 11), a Zn LMM peak at 991.3 eV, which appeared ~1 eV lower than the metallic Zn in CuZn, emerged in the hydrous condition and maintained its intensity at elevated temperatures. This peak was also observed when exposing CuZn alloy surface to 0.03 mbar H_2O at 300 K, and was assigned to $Zn_3(OH)_3$. AP-XPS measurements demonstrated the existence and thermal stability of $Zn_3(OH)_3$ species in $CO_2/H_2/H_2O$ at 550 K.

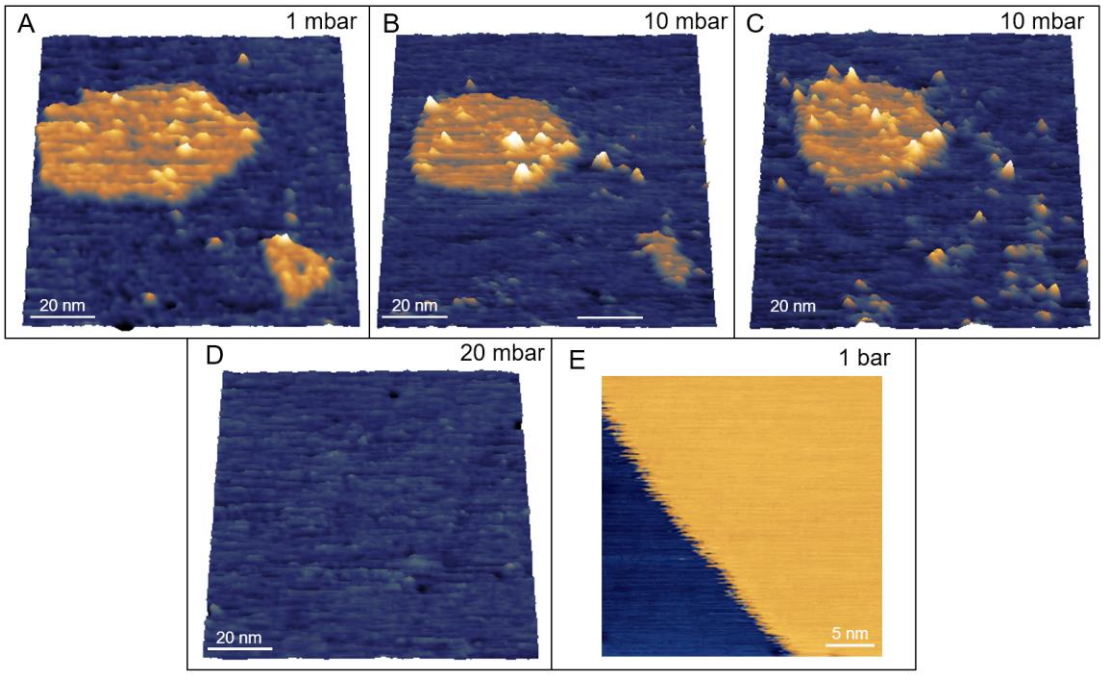

Supplementary Fig. 22 | Pressure-dependent ZnO decomposition dynamics. HP-STM images demonstrating the morphological evolution of ZnO islands on Cu(111) under varying pressures of CO_2/H_2 (1:3) gas mixtures with 0.04 mbar H_2O at 473 K. ZnO islands persisted on the CuZn alloy surface at (A) 1 mbar, but started to decompose progressively from edges at (B, C) 10 mbar. The smallest clusters observed displayed a size ~2 nm. ZnO islands decomposed completely (D) in 20 mbar mixture gases. At higher pressures, HP-STM shows the same surface morphology as (D) with exposed Cu terraces as exemplified (E) in 1 bar $CO_2/H_2/H_2O$ mixture gas (p_{CO_2} = 0.25 bar, p_{H_2} = 0.75 bar, p_{H_2O} = 3 mbar).

$$Zn_{3x}O_{3x-y}(OH)_{2y} + 1.5xH_2 \rightarrow xZn_3(OH)_3 + yH_2O$$

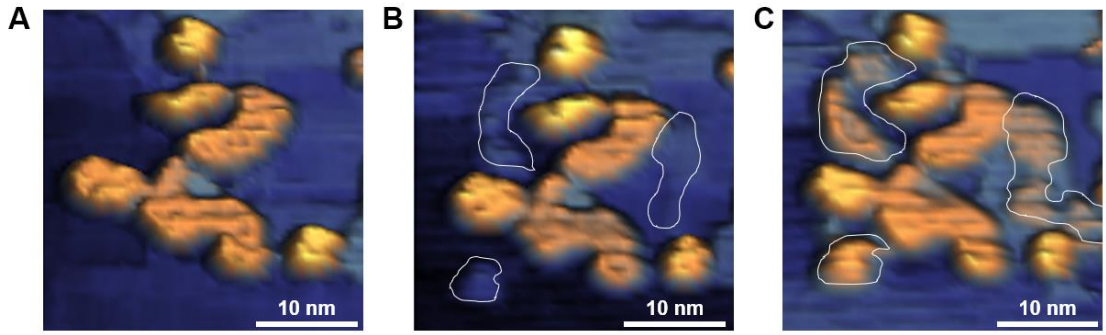

Supplementary Fig. 23 | Water-induced population of 3D ZnO particles. (A-C) HP-STM images showing the population of 3D ZnO particles on a CuZn alloy surface at 500 K in 5 bar CO_2/H_2 upon the addition of 30 mbar H_2O.

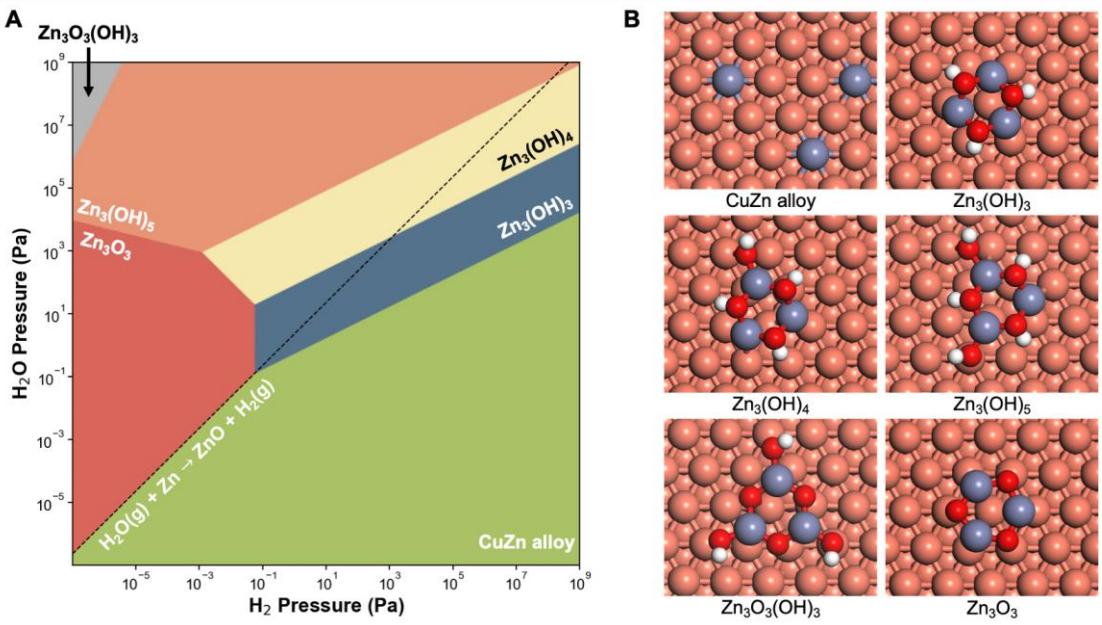

Supplementary Fig. 24 | DFT calculations for CuZn alloy oxidation by H_2O. (A) Phase diagram of ZnO_xH_y species, including CuZn alloy, $Zn_3(OH)_3$/Cu(111), $Zn_3(OH)_4$/Cu(111), $Zn_3(OH)_5$/Cu(111), $Zn_3O_3(OH)_3$/Cu(111), and Zn_3O_3/Cu(111), under varying H_2O and H_2 pressures at 473 K. Dashed black line indicate the equilibrium pressure of H_2 produced from H_2O dissociation. Conditions: T = 473 K. (B) Top views of DFT-optimized structures for species involved in the phase diagram. Color code: Reddish-orange – Cu; Cyan – Zn; Red – O; Gray – C; White – H.

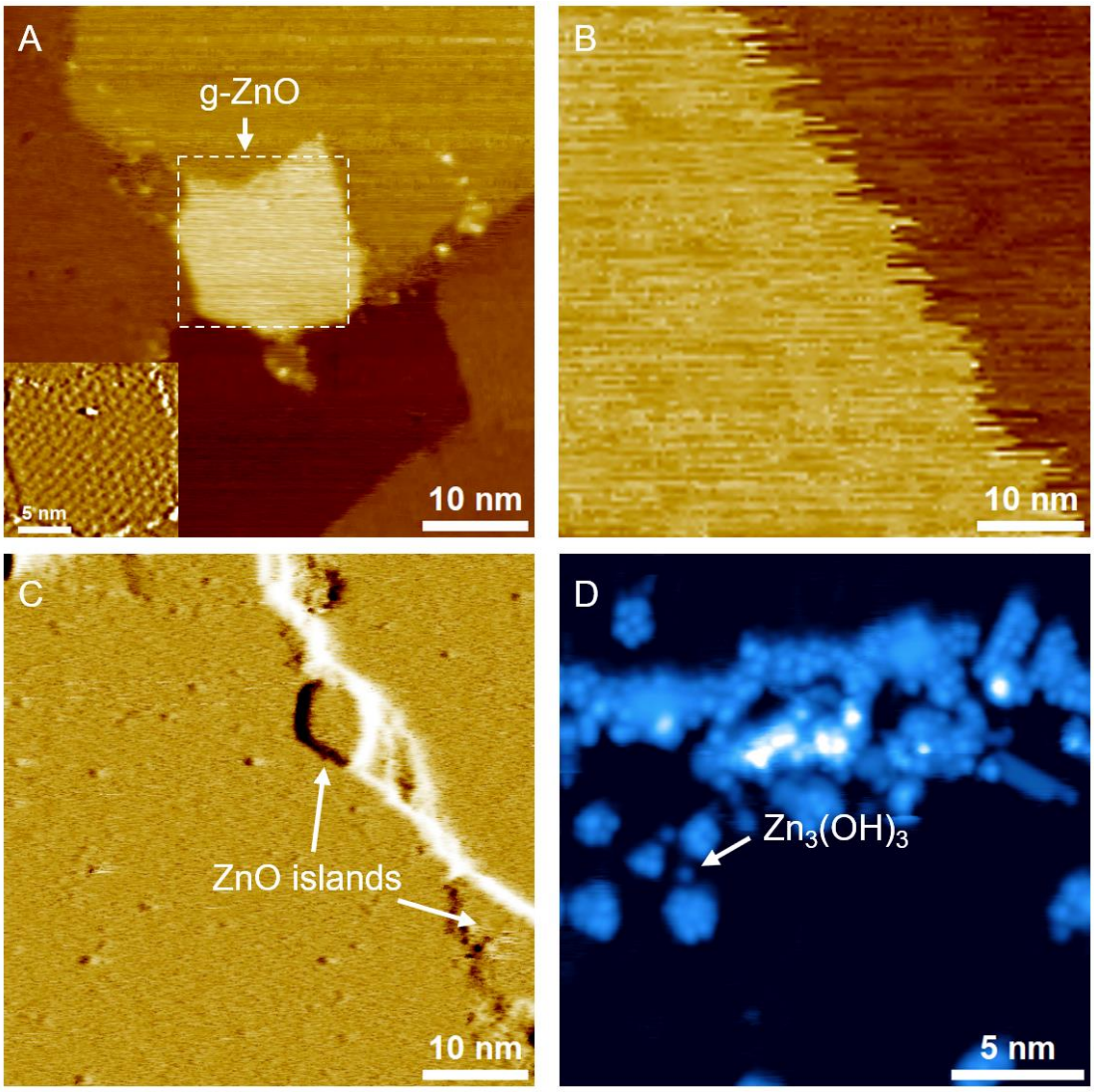

Supplementary Fig. 25 | High-pressure STM of ZnO/Cu(111) in 5 bar $CO_2/H_2/H_2O$. (A) STM image of as-prepared g-ZnO/Cu(111). (B) HP-STM image in 5 bar $CO_2/H_2/H_2O$ (p_{CO_2} = 1.25 bar, p_{H_2} = 3.75 bar, p_{H_2O} = 15 mbar) at 450 K, showing that clean Cu terraces were observed, accompanying the disappearance of ZnO islands. (C) STM image post-cooling under reaction atmosphere showing the reappearance of ZnO islands. (D) LT-STM image at 5 K showing $Zn_3(OH)_3$ species and agglomerated Zn_3-based complexes formation under 5 bar $CO_2/H_2/H_2O$ (p_{CO_2} = 1.25 bar, p_{H_2} = 3.75 bar, p_{H_2O} = 15 mbar) at 550 K.

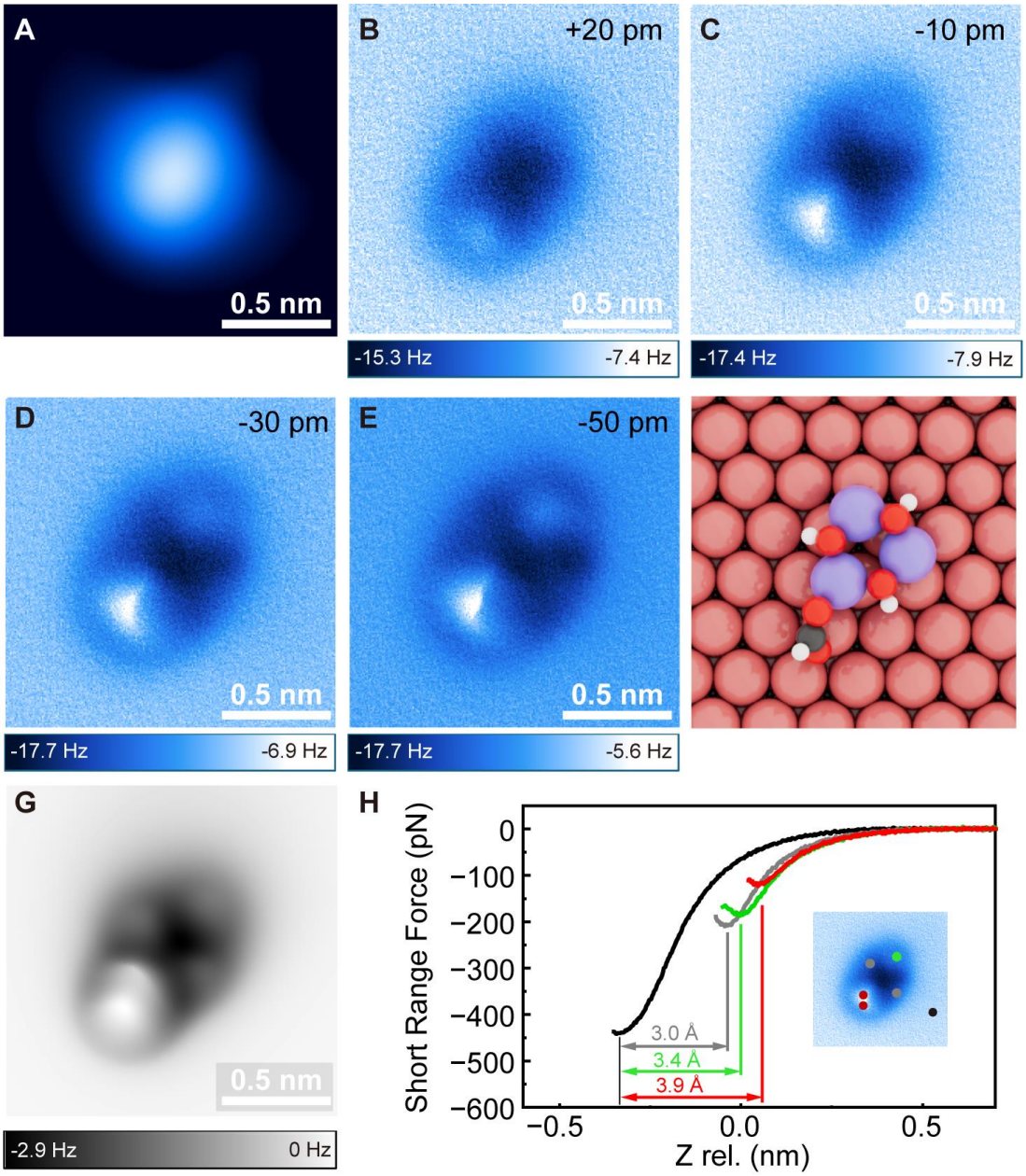

Supplementary Fig. 26 | Identification of $Zn_3(OH)_3(HCOO_i)$ on Cu(111) formed under 5 bar $CO_2/H_2/H_2O$ at 550 K. (A) STM and (B-E) constant-height AFM images of $Zn_3(OH)_3(HCOO_i)$ after exposing the CuZn alloy surface to 5 bar $CO_2/H_2/H_2O$ (p_{CO_2} = 1.25 bar, p_{H_2} = 3.75 bar, p_{H_2O} = 15 mbar) at 550 K. The tip heights of AFM images are +20 pm, -10 pm, -30 pm, -50 pm, respectively, which are referenced to the STM set point on Cu(111). Scanning parameters: V_s = 200 mV; I_t = 50 pA. (F) DFT-optimized model and (G) AFM simulation of the $Zn_3(OH)_3(HCOO_i)$. Color code: Reddish-orange - Cu; Cyan - Zn; Red - O; Gray - C; White - H. (H) Short-range force-distance curves for Cu(111) (black), bridge OH group (green and grey) and interfacial HCOO (red) showing the height profiles of $Zn_3(OH)_3(HCOO_i)$.

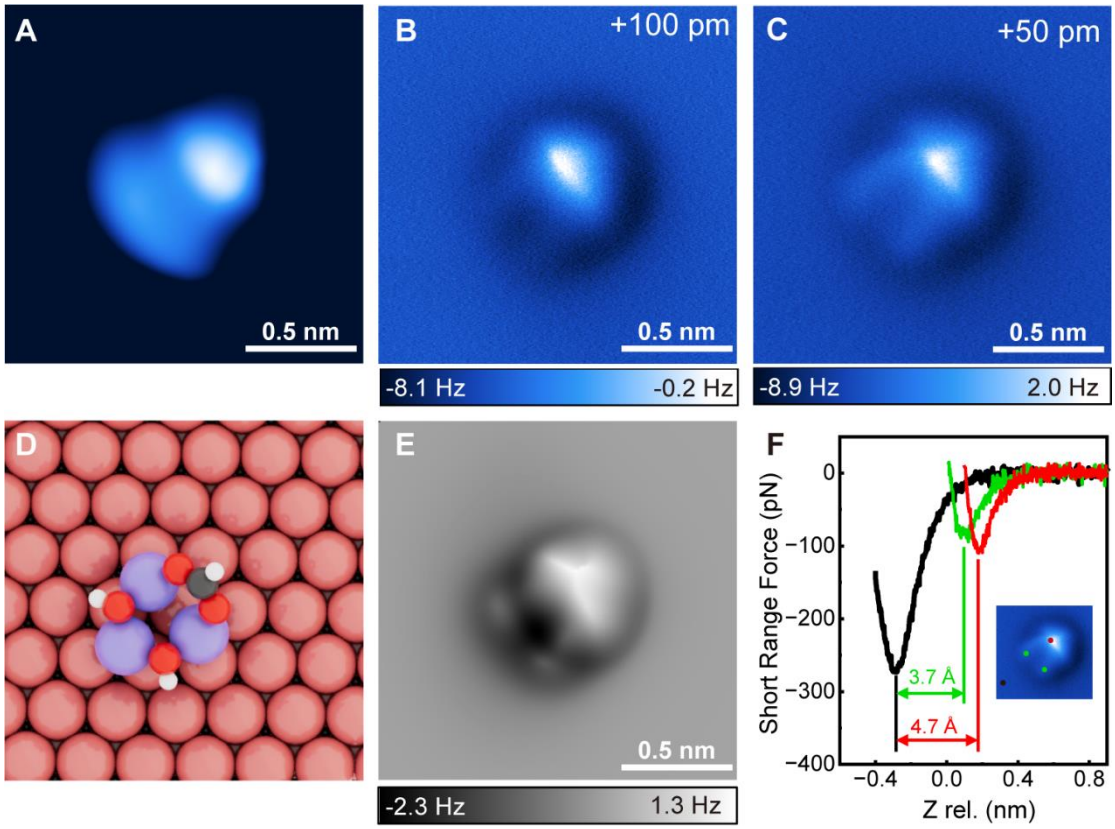

Supplementary Fig. 27 | Identification of $Zn_3(OH)_2(HCOO_b)$ on Cu(111). (A) STM and (B-C) corresponding constant-height AFM images of $Zn_3(OH)_2(HCOO_b)$. The tip heights of AFM images are +100 pm, +50 pm, respectively, which are referenced to the STM set point on Cu(111). Scanning parameters: V_s = -20 mV; I_t = 30 pA. (D) DFT-optimized model and (E) AFM simulation of the $Zn_3(OH)_2(HCOO_b)$. Color code: Reddish-orange - Cu; Cyan - Zn; Red - O; Gray - C; White - H. (F) Short-range force-distance curves for Cu(111) (black), bridge OH (green) and bridge HCOO (red) ligands, showing the height profiles of $Zn_3(OH)_2(HCOO_b)$ with locations indicated by the dots on the inset image. These dots use the same color code as the force curves.

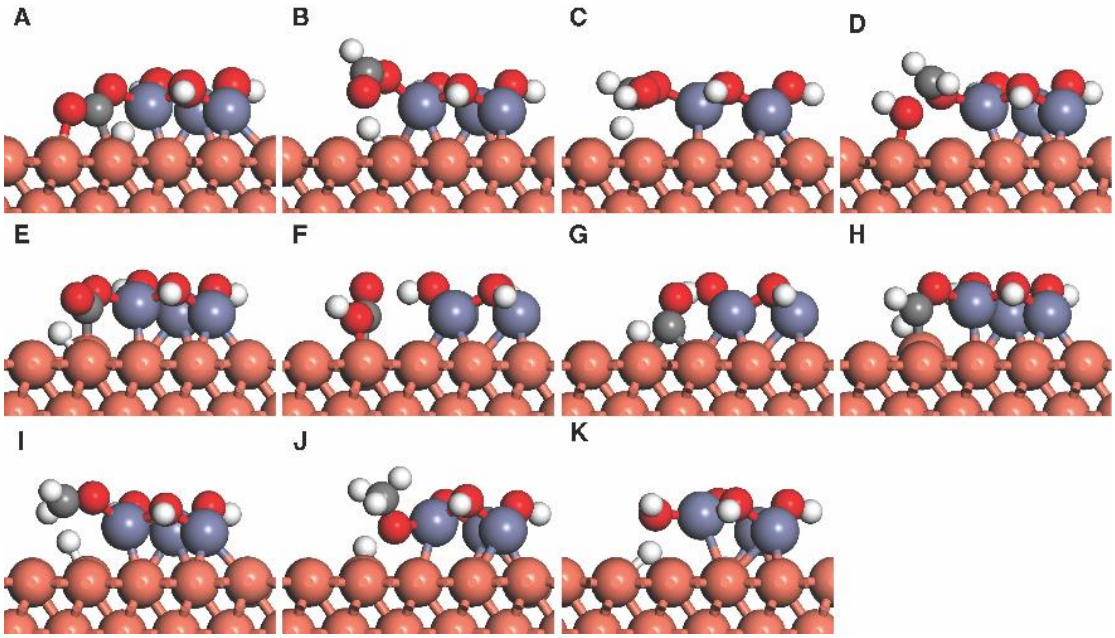

Supplementary Fig. 28 | DFT optimized transition states structures for elementary reactions in methanol synthesis from CO_2 hydrogenation over $Zn_3(OH)_3/Cu(111)$. (A) $*CO_2 + *H \rightarrow *HCOO_i + *$, (B) $*HCOO_i + *H \rightarrow *HCOOH + *$, (C) $*HCOOH + *H \rightarrow *H_2COOH + *$, (D) $*H_2COOH + * \rightarrow *CH_2O + *OH$, (E) $*CO_2 + *H \rightarrow *COOH + *$, (F) $*COOH + * \rightarrow *CO + *OH$, (G) $*CO + *H \rightarrow *CHO + *$, (H) $*CHO + *H \rightarrow *CH_2O + *$, (I) $*CH_2O + *H \rightarrow *CH_3O + *$, (J) $*CH_3O + *H \rightarrow *CH_3OH + *$, (K) $*OH + *H \rightarrow *H_2O + *$. Color code: Reddish-orange - Cu; Cyan - Zn; Red - O; Gray - C; White - H.

Supplementary Table 1 | DFT calculated reaction energies (ΔE, in eV) and activation barriers (Ea, in eV) for CO_2 hydrogenation over $Zn_3(OH)_3$/Cu(111), ZnO/Cu(111) [2], and ZnCu(211).[2]

Elementary reactions	$Zn_3(OH)_3$/Cu(111)		ZnO/Cu(111)†		ZnCu(211)†	
	ΔE	Ea	ΔE	Ea	ΔE	Ea
$CO_2(g) + * \rightarrow *CO_2$	-0.06	--	0.47	--	0.32	--
$CO(g) + * \rightarrow *CO$	-0.87	--	-0.65	--	-1.02	--
$CH_3OH(g) + * \rightarrow * CH_3OH$	-0.86	--	-0.64	--	-0.41	--
$H_2O(g) + * \rightarrow * H_2O$	-0.79	--	-0.58	--	-0.39	--
$*CO_2 + *H \rightarrow *HCOO_i + *$	-0.76	0.39	-0.83	0.18	-1.18	0.77
$*CO_2 + *H \rightarrow *HCOO_b + *$	-0.91	--	--	--	--	--
$*HCOO_b + *H \rightarrow *H_2COO_b + *$	0.58	--	--	--	--	--
$*HCOO_i + *H \rightarrow *HCOOH + *$	0.18	0.85	0.15	0.85	0.69	1.19
$*HCOOH + *H \rightarrow *H_2COOH + *$	-0.02	0.70	0.32	0.90	0.00	0.61
$*H_2COOH + * \rightarrow *CH_2O + *OH$	0.23	0.77	0.29	0.49	0.35	0.52
$*CO_2 + *H \rightarrow *COOH + *$	0.04	0.32	-0.11	0.73	-0.29	0.99
$*COOH + * \rightarrow *CO + *OH$	-0.24	0.62	0.19	0.84	-0.38	0.23
$*CO + *H \rightarrow *CHO + *$	0.34	0.66	0.39	0.88	0.41	0.73
$*CHO + *H \rightarrow *CH_2O + *$	-0.47	0.23	-0.59	0.25	-0.32	0.69
$*CH_2O + *H \rightarrow *CH_3O + *$	-0.88	0.13	-0.67	0.22	-1.07	0.12
$*CH_3O + *H \rightarrow *CH_3OH + *$	-0.32	0.55	-0.57	0.56	0.28	1.49
$*OH + *H \rightarrow *H_2O + *$	-0.39	0.61	-0.43	0.22	0.07	0.80

†: these values are reported in reference[2].

Captions for Supplementary Videos

Supplementary Video 1 | Video of in situ STM images showing the oxidation of a Zn/Cu(111) surface under 1×10^{-4} mbar H_2O at 300 K.

Supplementary Video 2 | Video of high-speed STM images of Zn/Cu(111) surface under 1×10^{-4} mbar H_2O with a scanning speed of 5 frames per second, showing the formation and migration of Zn_3-based complexes along step edges.

References

1 Barth, J. V., Brune, H., Ertl, G. & Behm, R. J. Scanning tunneling microscopy observations on the reconstructed Au(111) surface: Atomic structure, long-range superstructure, rotational domains, and surface defects. *Phys. Rev. B* **42**, 9307-9318 (1990). https://doi.org:10.1103/PhysRevB.42.9307

2 Kattel, S., Ramírez, P. J., Chen, J. G., Rodriguez, J. A. & Liu, P. Active sites for CO_2 hydrogenation to methanol on Cu/ZnO catalysts. *Science* **355**, 1296-1299 (2017). https://doi.org:10.1126/science.aal3573